Maya-Cornejo, J.; Garcia-Bernabe, A.; Compañ Moreno, V. (2018). Bimetallic electrocatalysts (Pt-M) supported on single-wall carbon nanotubes for hydrogen and methanol electrooxidation in fuel cells. International Journal of Hydrogen Energy. 43(2):872-884. https://doi.org/10.1016/j.ijhydene.2017.10.097

Bimetallic Pt-M electrocatalysts supported on single-wall carbon nanotubes for hydrogen and methanol electrooxidation in fuel cells applications

J. Maya-Cornejo[a], Abel Garcia-Bernabé[b], Vicente Compañ[b*]

[a] *Centro de Física Aplicada y Tecnología Avanzada, Universidad Nacional Autónoma de México, Querétaro, Qro, 76000, México.*

[b] *Departament de Termodinàmica Aplicada. Universitat Politècnica de València. Cami de Vera s/n 46022-València (Spain)*

**E-mail: vicommo@upv.es*

Abstract

A series of Pt-Ru and Pt-Mo bimetallic catalysts were prepared *via* a chemical reduction method by bubbling CO to form carbonyl compounds as metal precursors. In both cases the Pt-Ru and Pt-Mo bimetallic electrocatalysts achieved the maximum activity when the amount of Ru and Mo in the material was 50%wt. The physicochemical characterization of the electrocatalytic materials through X-ray diffraction (XRD) and transmission electron microscopy (TEM) has determined the presence of bimetallic structures. The electrochemical characterization using cyclic voltammetry, electrochemical impedance spectroscopy (EIS) and polarization curves in Proton Exchange Membrane Fuel Cells (PEMFC) and Direct Methanol Fuel Cell (DMFC) allowed to systematically investigate the electrocatalytic activity of the synthesized materials for the electrooxidation of hydrogen and methanol. The Pt-Ru/SWCNT electrocatalysts showed a higher current density at least 7-fold and 3-fold compared with Pt/SWCNT and Pt-Mo/SWCNT electrocatalysts, respectively. Besides, the Pt50%-Ru50%/SWCNT exhibited a shifting to negative values in the onset potential reaction for the electrooxidation of methanol of 200mV in comparison with Pt100%/SWCNT and Pt50%-Mo50%/SWCNT electrocatalysts. The experimental and simulated polarization curves obtained from DMFC show that Pt-Ru/SWCNT and Pt-Mo/SWCNT electrocatalysts exhibited higher power and current densities values compared with the Pt/SWCNT electrocatalyst. The membrane-electrode assembly (MEA) with Nafion® and the Pt-Ru/SWCNT electrocatalysts showed an open-circuit voltage value of 0.730V, significantly higher than that the values for the MEAs with Pt/SWCNT (0.663V) and Pt-Mo/SWCNT (0.633 V), respectively.

Keywords: Bimetallic electrocatalysts, electrochemical impedance spectroscopy (EIS), membrane-electrode assembly (MEA), fuel cell performance, PEMFC, DMFC.

1 Introduction

Proton-exchange membrane fuel cells (PEMFCs) are electrochemistry systems that convert chemical energy to electrical energy by means of the combustion of hydrogen, alcohols, hydrocarbons, etc., through the anodic reaction that is catalyzed at the anode where the fuel is inserted, while the oxygen is inserted into the cathode to complete the reaction [1]. Electrodes are generally porous gas diffusion electrodes to ensure the supply of reactant gases to active zones where the catalyst is in contact with the protonic membrane and the electronic (carbon) conductor. In the cathode, oxygen reduction reaction is normally catalyzed by platinum (Pt), where Pt dispersed on carbon exhibits a good performance. The oxidation reaction depends on the fuel, and the platinum is, in general, a good catalyst for this reaction. The platinum is important for oxidation of pure hydrogen. However, the presence of certain traces of gases such as CO, SO_2, H_2S, NO_2, NH_3 can poison the catalyst, which is particularly relevant in the case of CO for low temperature fuel cells. The CO molecules are prone to be adsorbed on the Pt catalyst surface, causing severe poisoning at low temperatures [2, 3]. Several strategies have been used to avoid CO contamination. Previous elimination of CO can be done by water-gas shift conversion of CO into CO_2 hereby producing more hydrogen. This conversion is favored at high temperature, but the equilibrium decreases with the H_2/CO ratio [3]. A similar strategy is the oxidation of CO by small amounts of air or oxygen, but the presence of the oxidant leads to a decrease in the fuel cell efficiency and raises a safety problem. The purification of the hydrogen before its insertion into fuel cells involves a great energetic cost for fuel cells. Stepwise reforming of hydrocarbons has been proposed for production of CO-free hydrogen for fuel cell applications [4]. The use of Pt alloys or ternary Pt-based catalysts have been widely studied to enhance CO tolerance.

The ability to dissociate the molecule of water at lowest potentials has been associated to ruthenium [5], in consequence, an anode that uses ruthenium can work at low potentials to obtain higher cell voltages only by re-formulating the Pt-based electrocatalysts [5]. Also, the use of a second metal as molybdenum has been reported to reduce the drawbacks associated to the CO adsorption on platinum electrocatalytic sites [6], because the effect of molybdenum is similar to that of ruthenium concerning the dissociation of

water to produce OH^- anions on their surface. These OH^- anions contribute to the oxidation of adsorbed species like CO carrying out their oxidation to CO_2 [7-9]. Some authors have proposed that the increase in the tolerance for CO poisoning in the Pt-Mo electrocatalyst is due to the oxygenated species formed by the molybdenum ($MoO(OH)_2$) [10, 11]. This species promotes the CO oxidation, which suggests that the increase in CO tolerance is achieved through a bifunctional mechanism [12]. Thus, there is a great interest in the study of Pt-M electrocatalysts, and the compositions studied include Pt-Ru [13-16], Pt-Mo [11, 17, 18], Pt-Ru-Mo [19] or Pt-Ru-X (X=Mo, Nb, Ta) [20]. Pt-Ru catalysts have been extensively used in direct methanol fuel cells (DMFC) [21]. CO is an intermediate specie in the methanol electro-oxidation and can occupy the active sites of the catalyst, resulting in slow reaction kinetics. With the use of ruthenium-platinum alloys the oxidation kinetics of methanol has improved significantly reaching a practicable level.

The majority of experimental studies focus the preparation of the electrocatalysts using carbon as support though of colloid based or different methods of impregnation [22, 23]. However the use of surfactant remains on the surface of the method colloid and hinders the fuel access to the catalyst sites [24]. The physics of carbon nanotubes have evolved rapidly since their discovery in 1991 of multi-wall carbon nanotubes and two years later the single-wall by Iijima [25]. Since then experimental studies have focused on different fields such as mechanics, optics and electronics due to excellent physical properties in various applications [25, 26]. From then carbon nanotube (CNT) based materials are been intensively studied due to a number of novel and unique properties that make them potentially useful in a wide range of applications. CNT layers offer outstanding properties like excellent flexibility, optical transparency, high electrical conductivity, extremely small weight, and low processing cost [27]. Single-walled carbon nanotubes can be described as a sheet of graphite that is rolled generating a cylindrical figure resulting in a structure in one dimension with axial symmetry. The diameters of single-walled carbon nanotubes lie in a range of 0.7 to 10.0 nm [28]. The structure of the CNT depends on the orientation of the hexagons in the cylinder with respect to the axis of the tube. As consequence of the orientation CNT have attracted much interest because they can former essentially one-dimensional periodic structures with electronic characteristics (metallic or semiconductor) and could be interesting to prepare MEAs using appropriate inks for fuel cells applications.

For their application, the catalysts are deposited on Gas Diffusion Layer (GDL), which permit the access of the combustion reactants to the catalysts and the electronic conduction. GDL are normally carbon. The proton-exchange membrane is placed between the anode and the cathode and is used as an electrolyte. Nafion® is the most studied and operated electrolyte for PEMFC's at low temperatures, having a sulfonated poly-tetrafluoroethylene polymeric structure. This membrane usually has a small temperature range in which it is stable. The upper limit of temperature is dictated by the humidification of the membrane, as water is a prerequisite for proton conduction.

In this work, we report the synthesis of Pt-Ru and Pt-Mo electrocatalysts supported on single-wall carbon nanotubes (SWCNT) for the electrooxidation of methanol and hydrogen in a proton-exchange membrane fuel cell (PEMFC). The characterization of the electrocatalytic materials was carried out by X-ray diffraction (XRD) and transmission electron microscopy (TEM) in order to determine the presence of a bimetallic structure. The electrochemical characterization was achieved using cyclic voltammetry, electrochemical impedance spectroscopy (EIS) and polarization curves in PEMFC and DMFC in order to systematically investigate the electrocatalytic activity of the synthesized materials for the electrooxidation of hydrogen and methanol.

Furtthermore, the experimental results obtained in PEMFC and DMFC were compared with the theoretically calculated parameters obtained by the use of the thermodynamic equations describing the behavior of the system and the resistance in the fuel cell arrangement.

2 Experimental

2.1 Synthesis of Pt-M bimetallic electrocatalysts

Metallic platinum was obtained from a precursor of H_2PtCl_6 that after weighing the desired amount was dissolved in 20 mL of distilled water. This dissolution was placed in a round-bottom two-necked flask to which CO was bubbled for about 12 hours under continuous stirring. During this process, the solution changed its color from orange to dark

purple with the formation of a dark precipitate. The changes in the dissolution are due to the formation of platinum carbonyl complexes ($[Pt_3(CO)_6]_n^{2-}$). When the bubbling of CO was stopped, and after a 30 minutes period to eliminate the residual CO in the flask, the single-wall carbon nanotubes support (Sigma-Aldrich, Batch #: 06905JH) was added to the dissolution previously dispersed in 1-2 dichlorobenzene (solvent). The mixture was heated to 90°C under continued stirring during 24 hours for the reduction of platinum. The final mixture was filtered and washed several times with diethyl ether.

In order to obtain the Pt-M electrocatalyst, during the platinum reduction reaction when the solution changes into a purple coloration (platinum carbonyl $[Pt_3(CO)_6]_n^{2-}$), the precursors of Ruthenium and Molybdenum ($Ru_3(CO)_{12}$ or $Mo(CO)_6$) was added to obtain the two different types of bimetallic electrocatalysts, subsequently the single-wall carbon nanotubes support was added into the dissolution previously dispersed in 1-2 dichlorobenzene (solvent). All the mixture was heated to 90°C in a continued stirring during 24 hours for the reduction of platinum and ruthenium or molybdenum. The final mixture was filtered and washed several times with diethyl ether. All the electrocatalysts were subjected to a thermal treatment at a temperature of 400°C for 2 hours in a cylindrical reactor in a N_2 atmosphere to remove the excess of organic solvents.

The synthesis of each electrocatalysts were prepared with the same theoretical amount of platinum (20%wt) owing we were want to studied the effect in the addition of different amounts of molybdenum and ruthenium.

2.2 Preparation of the working electrode for the half cell

To make an ink containing the electrocatalysts, 1.0 mg of catalyst, 10.0 µL of Nafion® and 100µL of isopropanol were mixed. The mixture was stirred in an ultrasonication bath water bath for 15 minutes, and then a 5.0 µL aliquot was taken and placed on the surface of a glassy carbon cylinder (0.785 cm^2) that had been previously dried for 10 minutes at room temperature.

2.3 Preparation of the membrane-electrode assembly

2.3.1 Electrocatalytic ink

The preparation of the electrocatalytic inks used to impregnate the GDL (Gas Diffusion Layer) was carried out using the catalysts previously synthesized in the laboratory, Nafion® dissolution as binder and isopropanol as solvent. The amount of electrocatalyst were used is related with an amount of platinum 1.5 mg cm^{-2} that impregnate on the GDL. The amount of electrocatalyst used was calculated according to each composition. The amount of Nafion® was 15%wt and that value has been take from the parametric investigations of direct methanol fuel cell electrodes manufactures by spraying, carried out by Koraishy et al. [29]. Also, the amount of isopropanol used was around 8 times higher than the combined amount of electrocatalyst and Nafion®. The surface of the GDL was 6.25 cm^2 and the impregnation of the ink was carried out by a suction type professional airbrush.

2.3.2 Activation of the proton exchange membrane

The proton-exchange membrane (Nafion® 117) was prepared in the laboratory using as precursor a dissolution of Nafion® (5.2% wt) supplied by DuPont via casting method. The Nafion® dissolution was placed in a flat-bottomed petri dish, which was then introduced in a climate chamber at 60 °C overnight to evaporate the solvent and produce the Nafion® membrane. After detachment from the petri dish, the thickness of the resulting membrane was measured with a HEIDENHAIN thickness instrument equipped with a flat tip. The results of the average thicknesses of membrane are presented in Table 1. The values shown there are the average of five measurements and the error included represents the standard deviation from the average value.

2.3.3 Membrane-Electrode Assembly

The membrane-electrode assembly (MEA) is formed by an anode, a cathode and the proton-exchange membrane. The anodes used were the GDL impregnate with our catalysts and their loadings are summarized in table 1. A commercial platinum-Black cathode was

directly with an amount of platinum of 1 mg cm^{-2} and the Nafion® 117 membranes were prepared.

The Nafion® 117 membrane was sandwiched between the anode and cathode electrodes, ensuring that the anode and cathode properly coincide. Later on, this assembly was placed in a hot press with a double metal plate (Rondol) to afford a proper binding of the two electrodes with the membrane. All the MEAs were prepared by this hot-press procedure working at 35 kg cm^{-2} and 130 ºC for 3 minutes.

Table 1 Composition (anode) and main properties of the prepared MEAs.

Sample	Electrocatalysts[a]	Pt loading (mg cm^{-2})	M loading (mg cm^{-2})	Thickness average (µm)	σ (S cm^{-1})
MEA1	$[Pt_{100\%}]_{20\%}/SWCNT_{80\%}$	1.5	-	202±8	$1.11x10^{-2}$
MEA2	$[Ru_{100\%}]_{20\%}/SWCNT_{80\%}$	-	1.5	193±8	$1.05x10^{-2}$
MEA3	$[Mo_{100\%}]_{20\%}/SWCNT_{80\%}$	-	1.5	200±10	$8.31x10^{-3}$
MEA4	$[Pt_{50\%}Mo_{50\%}]_{40\%}/SWCNT_{60\%}$	0.75	0.75	192±7	$1.67x10^{-2}$
MEA5	$[Pt_{67\%}Mo_{33\%}]_{30\%}/SWCNT_{70\%}$	1.0	0.5	206±7	$7.85x10^{-3}$
MEA6	$[Pt_{80\%}Mo_{20\%}]_{25\%}/SWCNT_{75\%}$	1.2	0.3	191±8	$8.73x10^{-3}$
MEA7	$[Pt_{80\%}Ru_{20\%}]_{25\%}/SWCNT_{75\%}$	1.2	0.3	194±8	$6.21x10^{-3}$
MEA8	$[Pt_{67\%}Ru_{33\%}]_{30\%}/SWCNT_{70\%}$	1.0	0.5	217±10	$8.47x10^{-3}$
MEA9	$[Pt_{50\%}Ru_{50\%}]_{40\%}/SWCNT_{60\%}$	0.75	0.75	212±9	$9.42x10^{-3}$

[a] Composition of the synthesized electrocatalysts used for the anode.

2.4 Physicochemical characterization

2.4.1 Transmission Electron Microscopy (TEM)

The technique of transmission electron microscopy (TEM) was used in order to observe the particle sizes present in the electrocatalyst. The microscope used was a JEOL JEM-2010 (available at USAI, Chemistry School, UNAM) using an acceleration voltage of 200 kV. From the images obtained by TEM it was possible to determine the average particle size.

2.4.2 X-ray Diffraction

This technique was used in order to know the metal phases present in the electrocatalysts as well as the possible presence of metal oxides. The equipment used for X-ray diffraction was a Siemens D5000 powder diffractometer (available at USAI, Chemistry School, UNAM) with a Cu Ka radiation source (λ=1.540562 Å). The 2θ range studied was $5° \leq 2\theta \leq 90$ degrees.

2.5 Electrochemical characterization

2.5.1 Half-cell electrochemical characterization

The experiments were conducted without agitation, the electrolyte was deoxygenated with N_2 and the electrochemical cell was an arrangement of three electrodes connected to a Voltalab PST050 potentiostat. The voltamperometric tests were taken at room temperature with a sweep rate of 30 mVs^{-1}. A saturated calomel electrode (SCE) was used as the reference electrode and the results were converted to the normal hydrogen electrode (NHE) scale. The working electrode was a glassy carbon cylinder impregnated with an ink that contained the electrocatalysts, while the auxiliary electrode was a graphite bar. The electrolytes that were used during the electrochemical half-cell tests were the following:

- 0.5 M H_2SO_4 dissolution.
- 0.5 M in H_2SO_4 and 0.5 M in CH_3OH dissolution.

2.5.2. Electrochemical impedance spectroscopy (EIS).

The proton conductivity of the MEAS was measured by impedance spectroscopy at different temperatures in the frequency range of 10^{-2} to 10^{6} Hz using a Novocontrol Broadband Dielectric Spectrometer (Hundsangen, Germany) integrated by an SR 830 lock-in amplifier with an Alpha dielectric interface. The MEAs were previously equilibrated with distilled water and afterwards placed between two gold electrodes in a liquid parallel plate cell coupled to the spectrometer and incorporating deionized water (Milli-Q) to ensure fully hydrated state of the samples. The temperature was controlled by nitrogen jet

(QUATRO from Novocontrol) with a temperature error of 0.1 K during every single sweep in frequency.

2.5.3 MEA's electrochemical characterization

Once all MEA's were prepared, the next step was their evaluation in a fuel cell (Baltic Fuel Cells). The MEA was placed in the middle of two bipolar plates of graphite with conventional channels for the distribution of the fuel. Once the MEA was positioned between the two bipolar plates, the whole system was inserted inside a device that closed with air pressure (4 psi), after which the fuel cell was ready for its use. The fuel cell measurements in a single PEMFC were performed at 25ºC. The flow rates were 0.25 L min^{-1} for pure hydrogen and 0.5 L min^{-1} for pure oxygen at atmospheric pressure.

For the sake of comparison, the different MEAs were also tested for direct methanol fuel cell application (DMFC). For this, a 2 M methanol solution in water, pumped at a flow rate of 5 mL min^{-1} was used to feed the anode. The cathode was directly fed with oxygen gas at a flow rate of 150 mL min^{-1} and 1 atm of pressure. In this case the measurements were made at 50 ºC.

3 Results

3.1 Physicochemical characterization

All the physicochemical characterization were carried out only for the $[Pt_{80\%}Ru_{20\%}]_{25\%}/SWCNT_{75\%}$ and $[Pt_{67\%}Mo_{33\%}]_{30\%}/SWCNT_{70\%}$ electrocatalysts that they exhibited the best electrochemical performance in half-cell.

The XRD patterns for the Pt, Pt-Ru and Pt-Mo electrocatalysts are shown in Figure 1. The peaks located at 2θ = 38.8, 46.5, 67.6, and 81.3° represent a face-centered cubic structure for Pt and correspond to its (111), (200), (220) and (311) planes respectively [30-33] (JCPDS Card 04-0802), for the $[Pt_{100\%}]_{20\%}/SWCNT_{80\%}$ electrocatalyst. In the case of the $[Pt_{67\%}Mo_{33\%}]_{30\%}/SWCNT_{70\%}$ electrocatalyst, the peaks in their XRD pattern show a

similar structure with the observed located at the same 2θ values of the Pt/SWCNT electrocatalyst. However, the XRD patterns for the $[Pt_{80\%}Ru_{20\%}]_{25\%}/SWCNT_{75\%}$ electrocatalyst exhibited a shifting toward higher 2θ values in the peaks characteristic for a face-centered cubic structure and this can be related with a change in the lattice parameter [31, 34, 35]. The observed values were 2θ = 40.87, 47.22, 69.54 and 83.98° that correspond to the (111), (200), (220) and (311) planes, respectively. The XRD patterns for the Pt-Ru and Pt-Mo electrocatalysts did not show any peak characteristic for Ru and Mo as the peak related with the (110) plane for Mo has a similar 2θ value than the one for Pt, this overlap sesulting in a broader peak [36], and the crystallographic response of Ru can only be seen for Ru contents above 60% wt [35-37]. Furthermore, the peaks in the XRD patterns for the $[Pt_{80\%}Ru_{20\%}]_{25\%}/SWCNT_{75\%}$ and $[Pt_{67\%}Mo_{33\%}]_{30\%}/SWCNT_{70\%}$ are wide compared to the shape of the Pt / SWCNT peaks due to the presence of Pt in the crystalline structure of Ru and Mo as rich-phase of the alloy element [37, 38]. All the XRD patterns also exhibited peaks at 2θ = 26.42, 44.37, 51.57 and 76.12°, corresponding to the (002), (200), (220) and (311) planes of the SWCNT used as the support [34, 39-41].

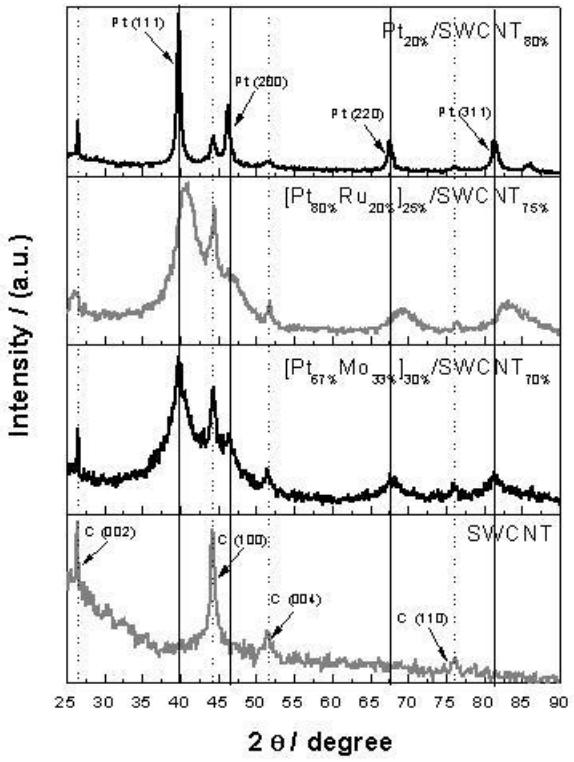

Figure 1 XRD patterns for the $[Pt_{80\%}Ru_{20\%}]_{25\%}/SWCNT_{75\%}$, $[Pt_{67\%}Mo_{33\%}]_{30\%}/SWCNT_{70\%}$, electrocatalysts along with those for $[Pt_{100\%}]_{20\%}/SWCNT_{80\%}$ and SWCNT.

The crystallite sizes were calculated using the Scherrer equation based on the corresponding (220) diffraction peak for each electrocatalyst and were determined to be 18, 7 and 15 nm for the $[Pt_{100\%}]_{20\%}/SWCNT_{80\%}$, $[Pt_{80\%}Ru_{20\%}]_{25\%}/SWCNT_{75\%}$ and $[Pt_{67\%}Mo_{33\%}]_{30\%}/SWCNT_{70\%}$ electrocatalysts, respectively. The lattice parameters calculated using the Bragg equation for the synthesized electrocatalysts along with the reported lattice parameters for commercial Pt/C are compared in Table 2. The lattice parameters for the Pt-Ru and Pt-Mo electrocatalysts showed a decrease in their value in comparison with commercial Pt values due to the alloying between Mo and Ru with Pt resulting in bimetallic nanoparticles for each electrocatalyst. This change in the lattice parameter is related with the shifting of the peaks in the XRD patterns [35, 42]. The wide peaks in the XRD patterns for the $[Pt_{80\%}Ru_{20\%}]_{25\%}/SWCNT_{75\%}$ and $[Pt_{67\%}Mo_{33\%}]_{30\%}/SWCNT_{70\%}$ and the change in each lattice parameter are related with the formation of an alloy [37, 38], discarding the formation of a physical mixture between Pt-M (M=Ru or Mo) [43].

Table 2 XRD parameters for the synthesized electrocatalysts.

Sample	Lattice parameter (Å)	Crystallite size (nm)
Pt/C commercial	3.9200 [31, 44]	15 [31]
$[Pt_{100\%}]_{20\%}/SWCNT_{80\%}$	3.9191	17
$[Pt_{80\%}Ru_{20\%}]_{25\%}/SWCNT_{75\%}$	3.8494	7
$[Pt_{67\%}Mo_{33\%}]_{30\%}/SWCNT_{70\%}$	3.9046	15

Figure 2 shows the STEM micrographs for the electrocatalysts synthesized. It can be observed that for $[Pt_{100\%}]_{20\%}/SWCNT_{80\%}$ (Fig. 2a), $[Pt_{80\%}Ru_{20\%}]_{25\%}/SWCNT_{75\%}$ (Fig. 2b) and $[Pt_{67\%}Mo_{33\%}]_{30\%}/SWCNT_{70\%}$ (Fig. 2c) the nanoparticles have a good distribution on the SWCNT support and those particles are displaying a homogeneous semi-spherical morphology. In relation to particle size, the average size obtained was 11 and 13 nm for the $[Pt_{100\%}]_{20\%}/SWCNT_{80\%}$ and $[Pt_{67\%}Mo_{33\%}]_{30\%}/SWCNT_{70\%}$ electrocatalysts, respectively, and 10 nm for the $[Pt_{80\%}Ru_{20\%}]_{25\%}/SWCNT_{75\%}$ electrocatalyst. Those results are consistent with

the crystallite sizes calculated using the Scherrer equation. Their chemical composition and the particles size distribution are presented in the supplementary information.

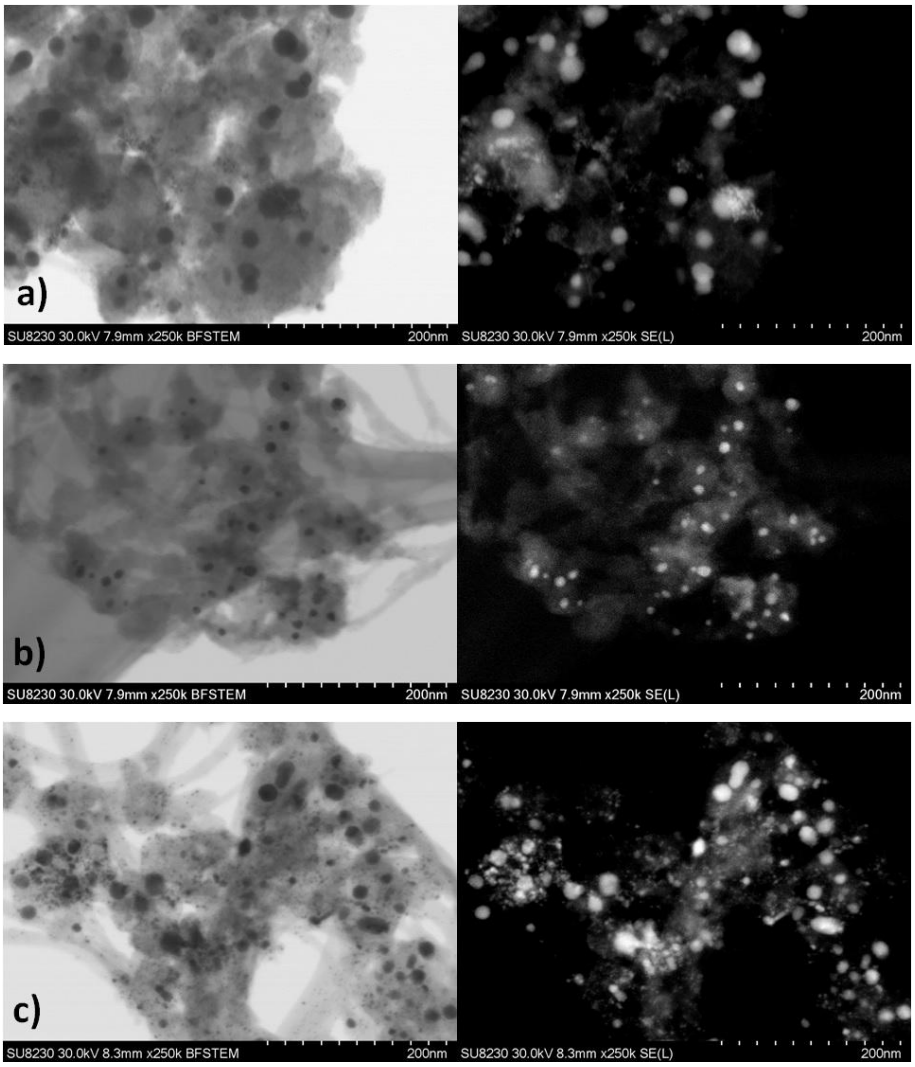

Figure 2 TEM micrographs for a) $[Pt_{100\%}]_{20\%}/SWCNT_{80\%}$, b) $[Pt_{67\%}Mo_{33\%}]_{30\%}/SWCNT_{70\%}$ and c) $[Pt_{80\%}Ru_{20\%}]_{25\%}/SWCNT_{75\%}$ electrocatalysts with Z contrast (right) and dark field (left).

3.2 Electrochemical characterization

The figure 3 shows the electrochemical response for the Pt-Ru/SWCNT (Fig. 3a) and Pt-Mo/SWCNT (Fig. 3b) electrocatalysts in acid media are comparable with the Pt/SWCNT electrocatalyst response. In the plot that corresponds to the Pt-Ru/SWCNT electrocatalyst (Fig. 3a) it is possible observe the classic response of a Pt material as it

exhibits the protons adsorption/desorption zone at 0.1 V *vs*. NHE, and the formation of platinum oxides around 0.9 V *vs*. NHE for the anodic sweep and the reduction of the platinum oxides between 0.85 and 0.4 V *vs*. NHE for the cathodic sweep. Furthermore, hydrogen formation on the Pt-Ru/SWCNT electrocatalyst happens at a single potential value and the shape of the peak is acute. This behavior is related with the affinity of the Pt-Ru/SWCNT electrocatalyst for the adsorption and formation of hydrogen. This feature indicates the possibility of using this material in a fuel cell for the electrooxidation of hydrogen. For the case of the Pt/SWCNT and Pt-Mo/SWCNT (Fig. 3b) electrocatalysts, the corresponding profiles did not show with clarity the formation and the reduction of platinum oxides. Also, the adsorption/desorption zone is not clear in both materials and for that reason the hydrogen evolution took place at lowest current densities.

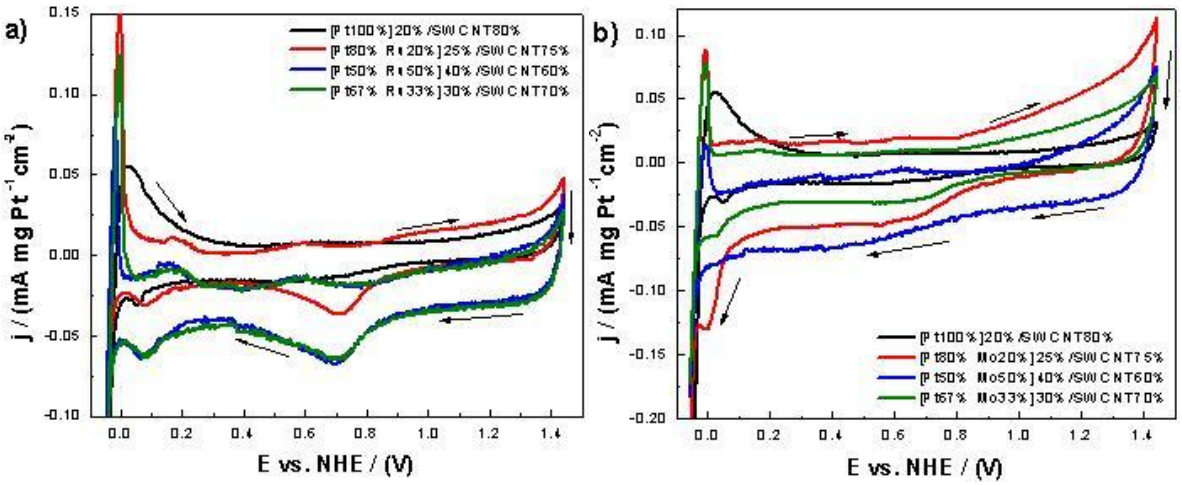

Figure 3 Cyclic voltammograms in 0.5 M H_2SO_4 for the Pt-M electrocatalysts at 30mV s^{-1}

To complement the electrochemical characterization, the Pt/SWCNT, Pt-Ru/SWCNT and Pt-Mo/SWCNT electrocatalysts were tested for the electrooxidation of methanol in acid media (Figure 4). The results revealed that the Pt-Ru/SWCNT electrocatalyst exhibited the highest electrocatalytic activity as the current density presented the highest value in comparison with the Pt/SWCNT and Pt-Mo/SWCNT electrocatalysts (at least a 7-fold and 3-fold increase, respectively) with the lowest amount of metal addition, providing a kinetic gain for the electrooxidation of methanol. Furthermore, for the Pt-Ru/SWCNT the onset potential reaction for the electrooxidation of methanol was shifted

towards negative potential (0.6 V *vs*. NHE) indicating that the oxidation reaction starts before in this electrocatalyst when compared with the Pt/SWCNT and Pt-Mo/SWCNT electrocatalysts, that exhibit an onset potential reaction of 0.8 V *vs*. NHE. Thus, this result shows that the Pt-Ru/SWCNT electrocatalyst achieves a thermodynamic gain for the electrooxidation of methanol in comparison with the other two materials and suggest that the Pt-Ru/SWCNT could be used as the anode in a DMFC.

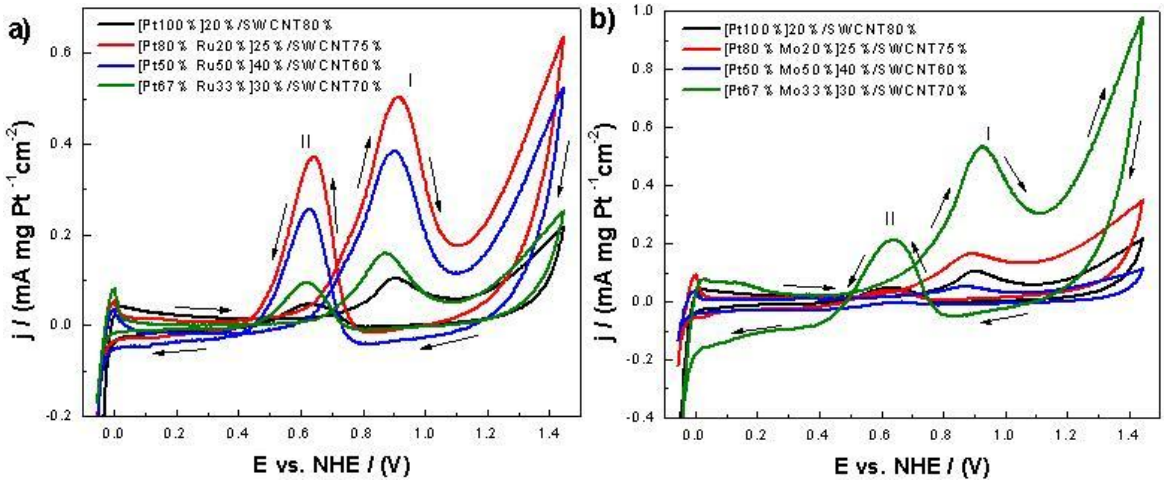

Figure 4 Electrooxidation of methanol 0.5 M in H_2SO_4 0.5 M

A final measurement was carried out to determine the degree of poisoning of the electrocatalysts. This can be calculated as the ratio between the peak current in the sweep forward i_f (Peak I) and the peak current in the sweep back i_b (Peak II). If the value of this ratio is above 1 this means that the electrocatalyst exhibits a high tolerance for the carbonaceous species that adsorb on their surface and shows an appreciable effectiveness to remove the adsorbed species that can poison the electrocatalyst [29, 31, 42-45]. For the present materials, the obtained ratios were 2.6, 1.2 and 5 for Pt/SWCNT, Pt-Ru/SWCNT and Pt-Mo/SWCNT, respectively, revealing that the three electrocatalysts have a quite good tolerance to carbonaceous species, avoiding the poison of their active sites, in particular for Pt-Mo/SWCNT.

3.3. Electrochemical impedance spectroscopy characterization

Electrochemical impedance spectroscopy (EIS) measurements were carried out at different temperatures in order to obtain information on the MEAs conductivity. The data of complex impedance were analyzed in terms of the corresponding Bode diagrams as shown in Figure 5. A close inspection of this figure shows that the modulus of the impedance decreases with the frequency until a constant value. However, the phase angle increases until a value close to 0º. The value of |Z*| constant means that the impedance has only a resistive contribution and its value represents the electrical resistance of the MEA. The capacity contribution of the impedance is more important at lower frequency. The slope of the modulus of impedance corresponds to the exponent of the frequency for a constant phase element (CPE), $Z^* = (i\omega C)^{-n}$. When the slope is one this corresponds to an ideal capacitor. Two different inclinations in the modulus of the impedance were observed, which can be related to different interface processes. Jeng *et al.* [49] applied an impedance model for MEAs with two CPEs that assigned to the electrode-membrane interface and the catalyst layer, respectively. These authors found that the exponents for the CPE at the interface are close to one, as in an ideal capacitor; however, the exponents for the CPE at the catalyst layer are around 0.6-0.7. The exponents found for the MEAs in the present study were between 0.85 and 0.45. The equivalent circuit for the electrical behavior of the prepared MEAs could be described as two CPEs and a resistance associated in series. The resistance for the MEA corresponds to the protonic resistance introduced by the Nafion® membrane together with the electronic resistance of the electrodes, being much higher the protonic resistance than the electronic resistance.

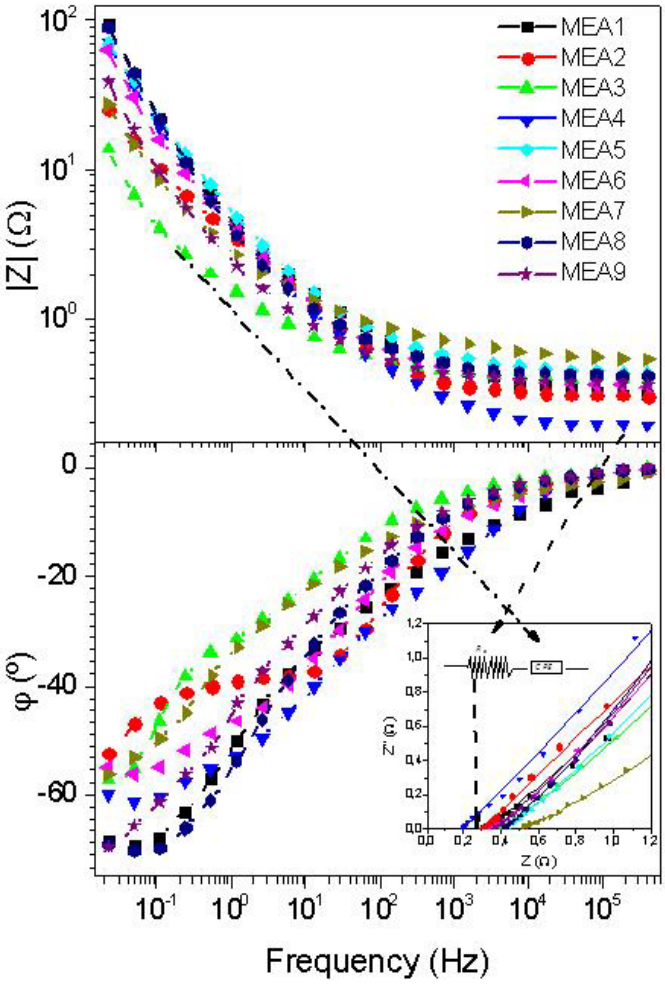

Figure 5. Bode diagram for all the MEAs at 25 ºC. The inset shows the Nyquist plots for the same MEAs at 25ºC. The points represent the experimental data while the continuous lines are the calculated fit by means of equivalent circuit shown in the plot.

In the inset of figure 5 we plot the imaginary part *vs*. the real part of the impedance for all the MEAs. In this plot, the so-called Nyquist diagram, the experimental data are represented as points and the solid lines represent the fitting curves obtained following the equivalent circuit commented above and indicated in the same inset. The resistance of the MEA can also be determined by the intersection of the Nyquist plot with the axis of abscissas, when Z'= R and Z" = 0. Is easy to probe that the values found are in agreement with the obtained by means of Bode diagram when the phase angle φ will be equal to 0.

The conductivity of the MEAs was calculated from the resistances by means of the expression

$$\sigma = \frac{l}{S\,R} \qquad (1)$$

where σ, S and l are, respectively, the proton conductivity, the area of the MEA and the thickness of the material that is in contact with the two gold electrodes in which we are making the measurements with the Novocontrol. The contact area was of 6.25 cm^2 for all MEAs, and the obtained proton conductivities are summarized in Table 3, showing an average value for the proton conductivity of $(9.7\pm1.2)\times10^{-3}$ S cm^{-1}. It is worth mentioning that the catalyst composition does not influence the proton conductivity for these MEAs. The SWCNT support has a high electronic conductivity; therefore, the electrical resistance of the electrode is very low compared with the resistance of Nafion® membrane.

3.4. Fuel cell performance

The performance of the different MEAs prepared with Nafion® membranes was measured in a single cell operating with H_2/O_2. They were evaluated over a long period of time at a constant voltage of 0.5 V. The resulting polarization curves at 25ºC and a high percentage of relative humidity are shown in Figure 6. An open circuit voltage (OCV) is near 1.0 V for all MEAs, which is a well-known typical value for Nafion® membranes. The cell voltage of a PEM fuel cell can be modeled by means of the equation (2) as reported by several authors [50-53],

$$V = V_{OC} - A_1 \cdot \ln\left(\frac{i}{i_0}\right) - i \cdot R \cdot S - m \cdot \exp(ni) \qquad (2)$$

where V is the cell voltage, Voc the reversible open circuit voltage, *i* the cell current density, i_0 the forward and reverse (exchange) current density at equilibrium under OC conditions, R is the protonic resistance of the membrane and S the area of the membrane exposed to the protons flux, m and n are empirical parameters associated with mass transport limitation phenomena. A is the sum of the slopes of the Tafel equation for anode

and cathode. The Tafel slope can be given by $A_1 = \frac{RT}{2\alpha F}$, where α is the charge-transfer coefficient, R the gas constant, T the absolute temperature and F the Faraday's constant. The fit of the equation (2) to the experimental values shown in Figure 6 can be used to obtain the values of Voc, A_1, i_0, R, m and n, respectively. For this purpose, the experimental results of the performance were fitted to the equation (2) using the GRG nonlinear algorithm and the fitting parameters are gathered in Table 3.

Table 3. Fitting parameters for the experimental I-V curves and maximum power density for all prepared MEAs

MEAs	Voc (V)	A (mV)	α	i_0 (mA cm^{-2})	R S (Ω cm^2)	m (V)	n (cm^2 mA^{-1})	P_{max} (mW cm^{-2})
MEA1	1.010	18.72	0.69	4.28x10^{-3}	0.36	3.18x10^{-2}	1.61x10^{-2}	66
MEA4	1.044	77.64	0.17	9.44x10^{-1}	0.65	8.87x10^{-5}	2.26x10^{-2}	107
MEA5	1.021	85.12	0.15	1.84	1.38	-	-	71
MEA6	1.025	49.20	0.26	2.27	0.39	8.15x10^{-2}	6.74x10^{-3}	88
MEA7	1.035	134.29	0.10	5.74	0.28	3.87x10^{-6}	3.17x10^{-2}	116
MEA8	1.037	18.92	0.68	3.48x10^{-3}	1.08	1.45x10^{-5}	2.96x10^{-2}	132
MEA9	1.007	74.21	0.17	1.49	0.28	3.19x10^{-3}	1.23x10^{-2}	125

A close inspection of the second term in equation (2) provides information on the activation losses, which are related with the charge-transfer coefficient (α parameter) describing the portion of the electrical energy applied that is employed in lowering the free energy barrier for the electrochemical reaction. The value of α must be in the 0-1 range. The value of 0.5 is accepted as a standard value for electrochemical reactions occurring in PEMFCs over platinum catalysts [54], but, in practical terms, values of α are used between 0.4 and 0.7 from experimental PEMFC's polarization curves [55-57]. The MEA8 with 33% of ruthenium in the catalyst has a very similar charge-transfer coefficient to MEA1 with only platinum at the catalyst. The presence of this percentage of ruthenium does not affect the catalytic activity for hydrogen combustion. Instead, the presence of molybdenum or other percentages of ruthenium reduce this catalytic activity [54, 55, 57]. The best values were observed for MEA1 and MEA8 with a very similar and low value. This indicates that

the substitution of 33% of platinum for ruthenium does not hinder the catalytic activity. The protonic resistance per unit of area, r (=R/S), depends both on the thickness and the protonic conductivity of the membrane. The protonic conductivity is affected by the relative humidity and not by the composition of catalyst. The last term of the equation (2) are the concentration losses that occur when the reactants are rapidly consumed at the electrodes by the electrochemical reactions taking place, leading to concentration gradients. The parameters m and n are empirical coefficients with typical values of 3×10^{-5} V and 8×10^{-3} cm^2 mA^{-1} [54, 55, 57]. The present results show typical values for MEA4, MEA7 and MEA8, and an acceptable value for MEA9. On the contrary, higher values were found for MEA1 and MEA6.

Figure 6 shows the evaluation of the synthesized electrocatalysts using a single PEMFC with the current-voltage and power curves for the oxidation of hydrogen. MEA1 was used as the reference because it only contains platinum. A comparison of the voltage that the MEAs achieved when the current density was 50 mA cm^{-2} showed the following trends: MEA8>MEA1≈MEA6≈MEA9≈MEA7>MEA4>MEA5. MEA8, with 33% of ruthenium, exhibited the highest cell voltage in comparison with other MEAs. However, the MEAs with different percentages of ruthenium (20% or 50%) or with some molybdenum (20%) afforded similar cell voltages to MEA1. For MEAs with a higher amount of molybdenum (33% or 50%), the cell voltages were worse. Power density in the PEMFC was obtained in the MEAs with Pt-Ru or Pt-Mo electrocatalysts as compared with MEA1 (Pt 100%). Furthermore, the MEAs using Pt-Ru electrocatalysts as anodes displayed higher power density values than the MEAs with Pt-Mo electrocatalysts, in particular MEA 8, with 33% of ruthenium, which presented the highest power density value (132 mW cm^{-2}). The results of the current densities for all the MEAs evaluated exhibited the same trends than the power density results, with the Pt-Ru electrocatalysts showing higher current density values than Pt-Mo and Pt electrocatalysts. Indeed, the highest current density value (350 mA cm^{-2}) was obtained for MEA9 (Pt50%-Ru50%). This was an expected behavior for the Pt-Ru/SWCNT electrocatalysts because they exhibited in the voltammograms an affinity for the hydrogen. For the Pt-Mo/SWCNT electrocatalysts, current densities values vary between 225 mA cm^{-2} (MEA5) and 325 mA cm^{-2} (MEA4) depending of Mo concentration, where the maximum power density obtained are compressed between 71

mW cm^{-2} in case of MEA5 (Pt67%-Mo33%) and 107 mW cm^{-2} for MEA4 (Pt50%-Mo50%). These values were higher than those for the Pt/SWCNT electrocatalyst. The increase in the performance of the PEMFC using the Pt-Ru/SWCNT and Pt-Mo/SWCNT electrocatalysts, over the Pt/SWCNT electrocatalyst, must be associated to the addition of Ru and Mo leading to a bimetallic material with modified surface properties, which is particularly relevant for the transition metals in combined with a noble metal [42, 58-60].

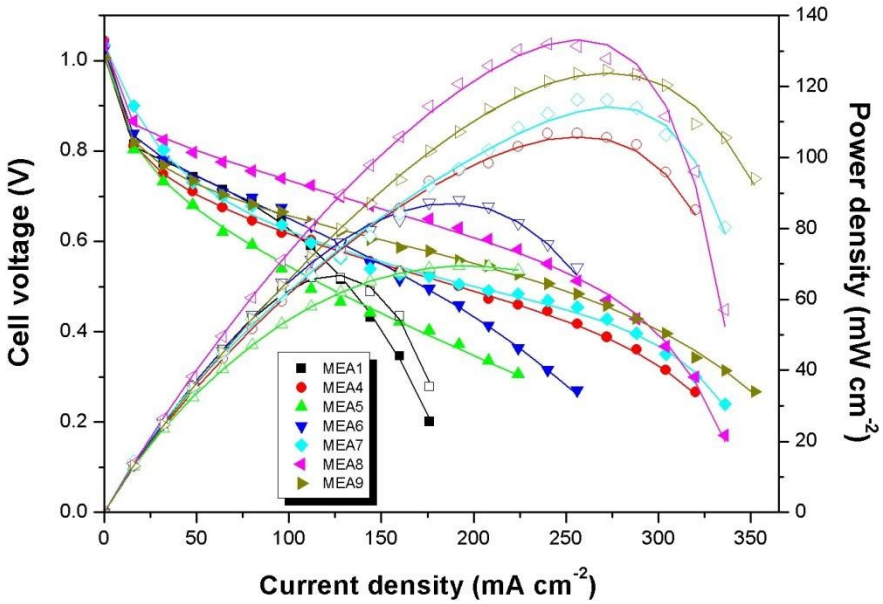

Figure 6. Polarization curves of MEAs with a Nafion® membrane and Pt/Ru or Pt/Mo at the anode under H_2/O_2 operation at 25ºC. Experimental data are represented by points and the continuous lines are obtained by fitting the data to the equation (2). The curves V *vs*. i are given by solid symbols and the curves of power densities *vs*. current density by open symbols.

To complement the electrochemical characterization, MEA1 (Pt/SWCNT), MEA9 (Pt-Ru/SWCNT) and MEA4 (Pt-Mo/SWCNT) were also tested in a single cell operating with $MeOH/O_2$ to know the performance of the MEAs in a direct methanol fuel cell (DMFC). Figure 7 shows the polarization curves at 50ºC with a 2 M methanol feed at the anode and pure oxygen without humidification in the cathode. As expected, the open circuit voltage (OCV) of the cell usually does not reach the theoretical value of the overall reversible cathode and anode potential at the given temperature and pressure.

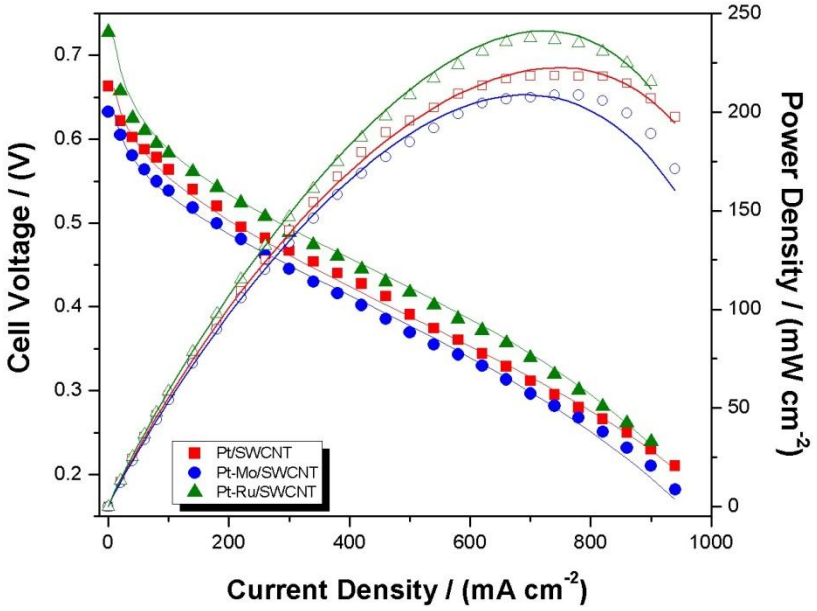

Figure 7. Polarization curves for the DMFC performance for the MEA 1 (Pt/SWCNT), MEA 4 (Pt50%-Mo50%/SWCNT) and MEA 9 (Pt50%-Ru50%/SWCNT) at 50ºC. Experimental data are represented by points and the continuous lines are obtained by fitting to the equation (2). The curves V *vs*. *i* are given by solid symbols and the curves of power densities *vs*. current density by open symbols.

The reduction of the OCV from the theoretical voltage has been attributed to the penetration of the fuel across the membrane and the catalyst [54, 61], and thus, these values are an indicator of the degree of methanol crossover by diffusion. The OCV value of the MEA9 of Nafion® with the Pt50%-Ru50%/SWCNT electrocatalyst is 0.730V, higher than the OCV for MEA1 (Pt100% /SWCNT, 0.663V) and MEA4 (Pt50%-Mo50%/SWCNT, 0.633V). These values are higher than the values found by Ren *et al.* [59] reporting OCV values around 0.6 V with S-ZrO2/ Nafion® membranes in DMFCs. They are also better that those found by S. Molla *et al*. [62] using commercial GDL covered by a Pt/Ru (50:50) alloy with a catalyst loading of 5.0 mg cm^{-2}.

On the other hand, the conductivity values for these MEAs found from the resistance values shown in Table 4 from measurements in single cell PEMFC with methanol as feed are in agreement with the values obtained by electrochemical impedance spectroscopy (EIS), using both the Nyquist and the Bode plots. Although proton conductivities of the MEAs under these conditions were *ca.* 0.010 S cm^{-1}, around 1/3 of the one measured for pristine Nafion®, 0.032 S cm^{-1}, the values of MEAs resistance found in the ohmic region of the I-V curve (linear behavior between i=200 mA cm^{-2} and i=600 mA

cm^{-2}) was 0.08 Ohm for the Nafion® membrane. This value is smaller than the value found for our MEAs under PEMFC with hydrogen as feed. The reason for this much shorter difference in the ohmic resistance exhibited by the MEAs under real DMFC operation can be explained again by the fact that the Nafion® membrane accomplishes a lower methanol crossover.

The maximum power density for the present MEAs containing Nafion® was for the Pt50%-Ru50%/SWCNT electrocatalyst with a value of 237.6 mW cm^{-2}. This value is higher than the one displayed by the MEA containing Nafion® and Pt100%/SWCNT (209.2 mW cm^{-2}) and the related MEA with Pt50%-Mo50%/SWCNT (118.7 mW cm^{-2}). Those results were in good agreement with those from the half-cell voltammograms for the electrooxidation of methanol, where the highest electrocatalytic activity was shown by the Pt-Ru/SWCNT electrocatalyst that reported the maximum current density and a shifting in the onset potential to highest negative values. The higher power density detected for MEA9 can be related with its higher affinity for the adsorption of methanol in comparison with the other electrocatalytic materials. The results obtained in this work for polarization curves and power densities are better than the ones found for PVI/Pd modified membranes and Nafion® 115 membranes, where, at 80 ºC, the maximum power density reached the value of 160 and 140 mW cm^{-2} respectively [63], and quite similar to those for the Nafion® - polyvinyl alcohol (PVA) nanofibers composite membranes [62]. The present results are also around 33% higher than those for a 46 μm thickness pristine Nafion® MEA using commercial electrodes, covered by an Pt/Ru alloy (50:50, 5 mg cm^{-2} catalyst loading) together with a 20%wt of dry Nafion® ionomer; and for the cathode a 5 mg cm^{-2} catalyst loading of Pt pressed onto a GDL [64]. The results are also improved in comparison with the MEA used by Kim *et al.* where the authors prepared a MEA dispersing a commercial Pt black catalyst in alcohol containing Nafion®, where the catalyst ink was coated onto the GDL for cathode 5mg cm^{-2} of Pt and for anode Pt/Ru in the proportion of 1:1 [65].

Thus, taking into account the former data and comparisons, the performance of the Nafion® MEAs prepared in this work with a Pt-Ru/SWCNT electrocatalyst are a good candidate to be used as a proton conductive material between anode and cathode in DMFCs and also in the case of PEMFCs.

Finally the results presented in Figure 7 were modeled by equation (2), where the feed fuel in the anode is methanol 2M of concentration and oxygen in the cathode. In all the measurements, the single DMFC was thermostatized at 50ºC. The fit of the experimental i-V and i-P values to equation (2) was carried out using the minimum mean square error method, in order to obtain the corresponding parameters. The fitting parameters *A, i_0, R, m* and *n* estimated are reported in Table 4 and the theoretical behavior according to these parameters is presented in Figure 8 by the solid lines included. As usual, the open circuit cell voltage, *V*, decreases from the thermodynamic electromotive force of the cell to a value between 0.63 and 0.73 V. As MEAs preparation has been the same in all cases and the membrane is the same (Nafion® of identical thickness) the abrupt decrease is caused in general by internal currents, energy activation of the oxidation reaction related with the electrodes catalyst loading and methanol crossover.

As can be observed, the value of *Voc* follows the trend *Voc* (MEA4) < *Voc* (MEA1) < *Voc* (MEA9). These differences can be attributed to the catalyst efficiency. The values of the proton resistance obtained from the experimental fit of the polarization curves were in agreement with the values measured directly by impedance spectroscopy in each MEA. Finally, the activation process associated with the electrocatalytic activity of the anode catalyst layer at the electrodes of MEAs through the values of the parameters i_0 and A_1 shows a better behavior of the MEA9 (Pt50%-Ru50%/SWCNT) than MEA1 (Pt100%/SWCNT) and MEA4 (Pt-Mo/SWCNT), respectively, at it is shown in table 4, where the presence of the Ruthenium at 50% in the catalyst decrease around of 25% the charge-transfer coefficient (α), in comparison with the other MEA's and the exchange current density vary from 8 mA cm^{-2} for MEA9 to 10 mA cm^{-2} and 14 mA cm^{-2} for MEA1 and MEA4, respectively.

Table 4 Fitting parameters for the i-V curves of MEA1 (anode of Pt100%/SWCNT), MEA9 (anode of Pt50%-Ru50%/SWCNT) and MEA4 (anode of Pt50%-Mo50%/SWCNT) using 2 M methanol solutions at 50ºC.

Samples	**Voc (V)**	**i_0 (mA cm^{-2})**	**A_1 (mV)**	**R (Ω)**	**m (V)**	**n (A^{-1})**	**α**
MEA1	0.663	10	36	0.053	0.00013	1.24	0.39

MEA4	0.63	14	34	0.031	0.007	0.63	0.28
MEA9	0.73	8	46	0.030	0.005	0.75	0.58

Thus, the Pt-Ru electrocatalyst (MEA9) showed the highest values of current densities and power density in comparison with the Pt-Mo and Pt100% electrocatalysts in DMFCs applications.

Finally, the overpotential due to the sum of the protonic resistance of the membrane and the methanol electro-osmotic effects was estimated following the procedure previously described by Li-Ning Huang *et al* [66]. For this, it can be assumed that the dV/di derivative, when the concentration of the methanol in the anode is constant, can be given as [62, 67].

$$\frac{dV}{di} = -\frac{A_2}{i} - A_3 \qquad (3)$$

Taking into account that at current densities above 200 mA cm^{-2}, $\frac{A_2}{i} < \frac{A_2}{150} << A_3$, then the first term in equation (3) can be omitted and the parameter A_3 calculated from the slope of the plot of V *vs*. i for current densities i> 150 mA cm^{-2} such as those observed from Figure 7, where the methanol crossover can be attributed to two mechanisms: electro-osmosis and diffusion. From data in Figure 8 and applying the equation (3) in the 200-600 mA cm^{-2} range the parameter A_3 was estimated and from this value, together with equation 21 of reference [62], $\chi \cdot J_{eos}$ can be obtained using equation (4) [66]

$$A_3 = \frac{L}{\sigma} + \chi \cdot J_{eos} \qquad (4)$$

where L is the thickness of the MEA, σ its conductivity and $\chi \cdot J_{eos}$ the resulting parameter relates the overpotential to a combination of protonic resistance (i.e. L/σ) and methanol crossover by electro-osmosis. The values obtained for the MEA with MEA9 (Pt50%-Ru50%/SWCNT), MEA1 (Pt100%/SWCNT) and MEA4 (Pt50%-Mo50%/SWCNT) were 3.7x10^{-4}, 3.5x10^{-4} and 3.3x10^{-4} V cm^2 mA^{-1}, respectively. From this result it can be observed that the parameter A_3 are quite similar but decreases in each MEA depend of the

type of catalyst. These results can be related with the electrodeposition and the surface composition of the bimetallic Pt:M catalysts. The activity of this composition shows that methanol oxidation is higher in Pt:Ru than in the other materials and higher than for a commercial catalyst with a 1:1 Pt:Ru bulk atomic ratio. Table 5 shows a comparison between the performances of our electrocatalysts with previous works reported performances.

Table 5. Performances of Pt /SWCNT, Pt-Ru/SWCNT and Pt-Mo/SWCNT electrocatalysts in compared with the literature.

Sample	Electrocatalyst		Fuel		Parameters			
	Anode	Cathode	Anode	Cathode	OCV (V)	Current density (mA cm^{-2})	P_{max} (mW cm^{-2})	Temp (°C)
MEA1	Pt/SWCNT	Pt/C	MeOH 2M	O_2	0.652	950	200	50
MEA4	Pt-Mo/SWCNT	Pt/C	MeOH 2M	O_2	0.640	950	210	50
MEA8	Pt-Ru/SWCNT	Pt/C	MeOH 2M	O_2	0.725	950	230	50
Kim [68]	Pt/C	Pt/C	H_2	Air	0.95	1400	****	80
Kim [38]	PtRu/C	Pt/C	H_2	Air	0.9	2000	450	70
Li [69]	Pt/C	Pt-Fe/C	MeOH 1M	O_2	0.7	400	****	90

The parameters that were obtained with the Pt/SWCNT, Pt-Ru/SWCNT and Pt-Mo/SWCNT electrocatalysts are close to the performance of the Kim et al. [68] even though in their research they used hydrogen as fuel and a higher temperature (80°C) in compared with our test (fuel: methanol 2M and 50°C). Furthermore, Li et al. [69] exhibited a lowest performance in their fuel cell because they obtained a low open circuit voltage (OCV), maximum power density and maximum current density with a temperature of 90°C in compared with our performance in a single direct methanol fuel cells at 50ºC. In conclusion, such is shown in table 5, our materials present an excellent performance for the electrooxidation of methanol using SWCNT as supported. In studies on DMFC our results show a power density using Pt/C in the cathode twice than obtained by Li at al. [69] using Pt-Fe/C as electrocatalysts in the cathode. On the other hand, the OCV is about 5% higher

in our MEAs using electrocatalysts of Pt/Ru in anode and Pt/C in the cathode than Pt-Ru/C in the anode and Pt-Fe/C in the cathode obtained by Li at al. [69].

4 Conclusions

The synthesis of bimetallic Pt-Ru and Pt-Mo electrocatalysts via chemical reduction by carbonyl compounds was successfully, obtaining semi-spherical nanoparticles with small dimensions (10 nm, respectively). The nanoparticles were supported on single-wall carbon nanotubes in order to evaluate the electrocatalytic activity for the electrooxidation of hydrogen and methanol. The Pt-Ru/SWCNT and Pt-Mo/SWCNT electrocatalysts showed higher electrocatalytic activity than Pt/SWCNT electrocatalyst for the electrooxidation of the fuels tested here. This enhancement is related to the addition of Ru and Mo because the bimetallic material changes the properties on the surface, when it is combined transition metals with a noble metal. The Pt-Ru/SWCNT electrocatalysts exhibit an affinity for the adsorption and the formation of hydrogen that result in a good response for the electrooxidation of hydrogen in a fuel cell, when were used hydrogen as fuel. Moreover, the Pt-Ru/SWCNT electrocatalysts showed a higher current density at least 7-fold and 3-fold in compared with Pt/SWCNT and Pt-Mo/SWCNT electrocatalysts, respectively. Besides, the Pt50%-Ru50%/SWCNT exhibited a shifting to negative values in the onset potential reaction for the electrooxidation of methanol of 200mV compared with Pt100%/SWCNT and Pt50%-Mo50%/SWCNT electrocatalysts. All the electrocatalysts were tested as anodes in a PEMFC using hydrogen and methanol as fuels. The results were obtained showed that the Pt50%-Ru50%/SWCNT electrocatalyst exhibited a better performances in single fuel cell than the Pt50%-Mo50%/SWCNT and Pt100%/SWCNT electrocatalysts. In the PEMFC for the Pt50%-Ru50%/SWCNT electrocatalysts the OCV obtained with hydrogen and methanol were 1.007 V and 0.730 V, respectively. Furthermore, the power densities obtained were 132 and 237.6 mW cm^{-2} and the current densities were 350 and 910 mA cm^{-2} using hydrogen and methanol, respectively. These results for DMFC are better than the results obtained by Li at al. [69] using Pt-Fe/C as electrocatalyst in the cathode.

Acknowledgements

The authors gratefully acknowledge for the Mexican Council for Science and Technology (CONACYT) for the scholarship to the research stay at Polytechnic University of Valencia (Spain) and the School of Chemistry of National Autonomous University of Mexico (UNAM) for providing the necessary infrastructure for the development of a part of this work. This research has been supported by the ENE/2015-69203-R project, granted by the Ministerio de Economía y Competitividad (MINECO), Spain.

References

[1] Carrette L, Friedrich KA, Stimming U. Fuel Cells: Fundamentals and Applications Fuel Cells. 2001;1:5-39.

[2] Igarashi H, Uchida H, Suzuki M, Sasaki Y, Watanabe M. Removal of carbon monoxide from hydrogen-rich fuels by selective oxidation over platinum catalyst supported on zeolite. Appl Catal A-Gen. 1997;159:159-69.

[3] Kahlich MJ, Gasteiger HA, Behm RJ. Kinetics of the Selective CO Oxidation in H_2-Rich Gas on Pt/Al_2O_3. J Catal. 1997;171:93–105.

[4] Choudhary TV, Goodman DW. CO-free fuel processing for fuel cell applications. Catalysis Today. 2002;77:65–78.

[5] He Z, Chen J, Liu D, Zhou H, Kuang Y. Electrodeposition of Pt-Ru nanoparticles on carbon nanotubes and their electrocatalytic properties for methanol electrooxidation. Diam Relat Mater. 2004;13:1764–70.

[6] Samjeské G, Wang H, Löffler T, Baltruschat H. CO and methanol oxidation at Pt-electrodes modified by Mo. Electrochim Acta. 2002;47:3681-92.

[7] Kuznetsovz VV, Kalinkina, A. A., Pshenichkina TV. Electrochemical Properties of Composite Materials Based on Platinum Modified with Molybdenum Compounds. Russ J Electrochem. 2007;43:776-81.

[8] Ordóñez LC, Roquero P, Sebastian PJ, Ramírez J. Carbon-supported platinum-molybdenum electro-catalysts for methanol oxidation. Catalysis Today. 2005;107-108:46–52.

[9] Ordóñez LC, Roquero P, Sebastian PJ, Ramírez J. CO oxidation on carbon-supported PtMo electrocatalysts: Effect of the platinum particle size. Int J Hydrogen Energy. 2007;32:3147–53.

[10] Mikhailova AA, Pasynskii, A. A., Dobrokhotova ZV, Grinberg VA, Khazova OA. CO Oxidation at Platinum–Molybdenum Electrodes. Russ J Electrochem. 2008;44:303-12.

[11] Santiago EI, Bastida MS, Assaf EM, Ticianelli EA. Mechanism of CO Tolerance on Molybdenum-Based Electrocatalysts for PEMFC. J Electrochem Soc. 2004;151:A944-A9.

[12] Yoo E, Okada T, Kizuka T, Nakamura J. Effect of carbon substrate materials as a Pt–Ru catalyst support on the performance of direct methanol fuel cells. J Power Sources. 2008;180:221–6.

[13] Chang W-C, Nguyen MT. Investigations of a platinum–ruthenium/carbon nanotube catalyst formed by a two-step spontaneous deposition method. J Power Sources. 2011;196:5811–6.

[14] Cheng TTH, Jia N, Colbow V, Wessel S, Dutta M. Effect of gas composition on Ru dissolution and crossover in polymer-electrolyte membrane fuel cells. J Power Sources. 2010;195:4622–7.

[15] Modestov AD, Tarasevich MR, Filimonov VY, Davydova ES. CO tolerance and CO oxidation at Pt and Pt–Ru anode catalysts in fuel cell with polybenzimidazole–H_3PO_4 membrane. Electrochim Acta. 2010;55:6073–80.

[16] Sung L-Y, Hwang B-J, Hsueh K-L, Su W-N, Yang C-C. Comprehensive study of an air bleeding technique on the performance of a proton-exchange membrane fuel cell subjected to CO poisoning. J Power Sources. 2013;242:264-72.

[17] Ioroi T, Akita T, Yamazaki S-i, Siroma Z, Fujiwara N, Yasuda K. Comparative study of carbon-supported Pt/Mo-oxide and PtRu for use as CO-tolerant anode catalysts. Electrochim Acta. 2006;52:491–8.

[18] Ioroi T, Yamazaki S-i, Siroma Z, Fujiwara N, Yasuda K. Electrochemical impedance study of carbon-supported Pt/Mo-Oxide for CO-Tolerant anode catalyst. Electrochemistry. 2007;75:159-62.

[19] Benker N, Roth C, Mazurek M, Fuess H. Synthesis and Characterisation of Ternary Pt/Ru/Mo Catalysts for the Anode of the PEM Fuel Cell. J New Mater for Electrochem Systems 2006;2:121-6.

[20] Papageorgopoulos DC, Keijzer M, de Bruijn FA. The inclusion of Mo, Nb and Ta in Pt and PtRu carbon supported 3electrocatalysts in the quest for improved CO tolerant PEMFC anodes. Electrochim Acta. 2002;48:197-204.
[21] Liu H, Song C, Zhang L, Zhang J, Wang H, Wilkinson DP. A review of anode catalysis in the direct methanol fuel cell. J Power Sources. 2006;155:95–110.
[22] Reich S, Thomsen C, Maultzsch J. Cabon Nanotubes. Basic Concepts and Physical Properties: Wiley-VCH; 2004.
[23] Loiseau A, Launois P, Petit P, Roche S, Salvetat JP. Undestanding Carbon Nanotubes for Basic to Applications: Springer; 2006.
[24] Anoshkin IV, Nefedova II, Lioubtchenko DV, Nefedov IS, Räisänen AV. Single walled carbon nanotube quantification method employing the Raman signal intensity. Carbon. 2017;116:547-52.
[25] Saito R, Dresselhaus G, Dresselhaus MS. Physical Properties of Carbon Nanotubes: Imperial College Press; 1998.
[26] Koraishy BM, Solomon S, Meyers JP, Wood KL. Parametric Investigation of Direct Methanol Fuel Cell Electrodes Manufactured by Spraying. J Fuel Cell Sci Tech. 2012;9:021003-1 - -5.
[27] Gao G, Yang G, Xu M, Wang C, Xu C, Li H. Simple synthesis of Pt nanoparticles on noncovalent functional MWNT surfaces: Application in ethanol electrocatalysis. J Power Sources. 2007;173:178–82.
[28] Maya-Cornejo J, Guerra-Balcázar M, Arjona N, Álvarez-Contreras L, Rodríguez Valadez FJ, Gurrola MP, et al. Electrooxidation of crude glycerol as waste from biodiesel in a nanofluidic fuel cell using Cu@Pd/C and Cu@Pt/C. Fuel. 2016;183:195-205.
[29] Mu Y, Liang H, Hu J, Jiang L, Wan L. Controllable Pt Nanoparticle Deposition on Carbon Nanotubes as an Anode Catalyst for Direct Methanol Fuel Cells. J Phys Chem B. 2005;109:22212-6.
[30] Yong L, Hao Y, Xiying L, Liqun M. Pt nanoparticles supported on monodisperse carbon spheres for methanol oxidation in alkaline media. Mater Lett. 2013;105:287–9.
[31] Li F, Guo Y, Chen M, Qiu H, Sun X, Wang W, et al. Comparison study of electrocatalytic activity of reduced graphene oxide supported Pt-Cu bimetallic or Pt

nanoparticles for the electrooxidation of methanol and ethanol. Int J Hydrogen Energy. 2013;38:14242-9.

[32] Sarkar A, Manthiram A. Synthesis of Pt@Cu Core-Shell Nanoparticles by Galvanic Displacement of Cu by Pt^{4+} Ions and Their Application as Electrocatalysts for Oxygen Reduction Reaction in Fuel Cells. J Phys Chem C. 2010;114:4725–32.

[33] Tang M, Nelson AT, Wood ES, Maloy SA, Jiang Y-B. Grazing incidence X-ray diffraction and transmission electron microscopy studies on the oxide formation of molybdenum in a water vapor environment. Scr Mater. 2016;120:49–53.

[34] Antolini E, Cardellini F. Formation of carbon supported PtRu alloys: an XRD analysis. J Alloy Compd. 2001;315:118-22.

[35] Kim I, Bong S, Woo S, Mahajan RK, Kim H. Highly active 40 wt.% PtRu/C anode electrocatalysts for PEMFCs prepared by an improved impregnation method. Int J Hydrogen Energy. 2011;26:1803-12.

[36] Ledesma-García J, Maya-Cornejo J, Arjona N, RIvas S, Álvarez-Contreras L, Guerra-Balcázar M, et al. Support Effect in the Electrocatalytic Activity of Cu@Pd Core-Shell toward Electrooxidation of Short Chain Alcohols in Alkaline Media. J Electrochem Soc. 2015;162:F1439-F44.

[37] Sebastián D, Lázaro MJ, Moliner R, Suelves I, Arico AS, Baglio V. Oxidized carbon nanofibers supporting PtRu nanoparticles for direct methanol fuel cells. Int J Hydrogen Energy. 2014;39:5414-23.

[38] Jeng K-T, Chien C-C, Hsu N-Y, Yen S-C, Chiou S-D, Lin S-H, et al. Performance of direct methanol fuel cell using carbon nanotube-supported Pt–Ru anode catalyst with controlled composition. J Power Sources. 2006;160:97–104.

[39] Maya-Cornejo J, Ortiz-Ortega E, Álvarez-Contreras L, Arjona N, Guerra-Balcázar M, Ledesma-García J, et al. Copper–palladium core–shell as an anode in a multi-fuel membraneless nanofluidic fuel cell: toward a new era of small energy conversion devices. Chem Commun. 2015;51:2536--9.

[40] Radmilovic V, Gasteiger HA, Ross-Jr PN. Structure and chemical composition of a supported Pt-Ru electrocatalyst for methanol oxidation. J Catal. 1995;154:98-106.

[41] Singh B, Dempsey E, Dickinson C, Laffirb F. Inside/outside Pt nanoparticles decoration of functionalised carbon nanofibers ($Pt_{19.2}$/f-$CNF_{80.8}$) for sensitive non-enzymatic electrochemical glucose detection. Analyst. 2012;1387:1639–48.

[42] Divya P, Ramaprabhu S. Platinum nanoparticles supported on a bi-metal oxide grown carbon nanostructure as an ethanol electrooxidation electrocatalyst. J Mater Chem A. 2013;1:13605–11.

[43] Kang WD, Wei YC, Liu CW, Wang KW. Enhancement of electrochemical properties on Pd–Cu/C electrocatalysts toward ethanol oxidation by atmosphere induced surface and structural alteration. Electrochem Commun. 2011;13:162-5.

[44] Long NV, Ohtaki M, Hien TD, Randy J, Nogami M. A comparative study of Pt and Pt–Pd core–shell nanocatalysts. Electrochim Acta. 2011;56:9133-43.

[45] Wang H, Wang R, Li H, Wang Q, Kang J, Lei Z. Facile synthesis of carbon-supported pseudo-core@shell PdCu@Pt nanoparticles for direct methanol fuel cells. Int J Hydrogen Energy. 2011;36:839-48.

[46] Jeng K-T, Chien C-C, Hsu N-Y, Huang W-M, Chiou S-D, Lin S-H. Fabrication and impedance studies of DMFC anode incorporated with CNT-supported high-metal-content electrocatalyst. J Power Sources. 2007;164:33–41.

[47] Kim J, Lee S-M, Srinivasan S, Chamberlin CE. Modeling of Proton Exchange Membrane Fuel Cell Performance with an Empirical Equation. J Electrochem Soc. 1995;142:2670-4.

[48] Laurencelle F, Chahine R, Hamelin J, Agbossou K, Fournier M, Bose TK, et al. Characterization of a Ballard MK5-E Proton Exchange Membrane Fuel Cell Stack. Fuel Cells. 2001;1:66-71.

[49] Mollá S, Compañ V, Gimenez E, Blazquez A, Urdanpilleta I. Novel ultrathin composite membranes of Nafion/PVA for PEMFCs. Int J Hydrogen Energy. 2011;26:9886-95.

[50] Pisani L, Murgia G, Valentini M, D'Aguanno B. A new semi-empirical approach to performance curves of polymer electrolyte fuel cells. J Power Sources. 2002;108:192-203.

[51] Larminie J, Dicks A. Fuel Cell System Explained. Chichester, England: John Wiley&Sons Ltd.; 2000.

[52] Danilov VA, Tade MO. An alternative way of estimating anodic and cathodic transfer coefficients from PEMFC polarization curves. Chem Eng J. 2010;156:496–9.
[53] Fernandez-Carretero FJ, Suarez K, Solorza O, Riande E, Compañ V. PEMFC Performance of MEAS Based on Nafion® AND sPSEBS Hybrid Membranes. J New Mater for Electrochemical Syst. 2010;13:191-9.
[54] Kunusch C, Puleston PF, Mayosky MA, Moré JJ. Characterization and experimental results in PEM fuel cell electrical behaviour. Int J Hydrogen Energy. 2010;35:5876-81.
[55] Bligaard T, Nørskov JK. Ligand effects in heterogeneous catalysis and electrochemistry. Electrochim Acta. 2007;52:5512-6.
[56] Hu S, Scudiero L, Ha S. Electronic effect on oxidation of formic acid on supported Pd–Cu bimetallic surface. Electrochim Acta. 2012;83:354-8.
[57] Hu S, Scudiero L, Ha S. Electronic effect of Pd-transitionmetal bimetallic surfaces toward formic acid electrochemical oxidation. Electrochem Commun. 2014;38:107-9.
[58] Chen L-C, Yu TL, Lin H-L, Yeh S-H. Nafion/PTFE and zirconium phosphate modified Nafion/PTFE composite membranes for direct methanol fuel cells. J Membr Sci. 2008;307:10-20.
[59] Mollá S, Compañ V. Performance of composite Nafion/PVA membranes for direct methanol fuel cells. J Power Sources. 2011;196:2699-708.
[60] Tian AH, Kim J-Y, Shi JY, Kim K. Poly(1-vinylimidazole)/Pd-impregnated Nafion for direct methanol fuel cell applications. J Power Sources. 2008;183:1-7.
[61] Mollá S, Compañ V. Polyvinyl alcohol nanofiber reinforced Nafion membranes for fuel cell applications. J Membr Sci. 2011;372:191-200.
[62] Kim TK, Kang M, Choi YS, Kim HK, Lee W, Chang H, et al. Preparation of Nafion-sulfonated clay nanocomposite membrane for direct menthol fuel cells via a film coating process. J Power Sources. 2007;165:1-8.
[63] Huang L-N, Chen L-C, Yu TL, Lin H-L. Nafion/PTFE/silicate composite membranes for direct methanol fuel cells. J Power Sources. 2006;161:1096-105.
[64] Gonzalez-Ausejo J, Cabedo L, Gamez-Pérez J, Molla S, Giménez E, Compañ V. Modification of Nafion Membranes with Polyaniline to Reduce Methanol Permeability. J Electrochem Soc. 2015;162:E325-E33.

[65] Kim K-H, Lee K-Y, Lee S-Y, Cho E, Lim T-H, Kim H-J, et al. The effects of relative humidity on the performances of PEMFC MEAs with various Nafion® ionomer contents. Int J Hydrogen Energy. 2010;35:13104-10.
[66] Li W, Zhou W, Li H, Zhou Z, Zhou B, Sun G, et al. Nano-stuctured Pt–Fe/C as cathode catalyst in direct methanol fuel cell. Electrochim Acta. 2004;49:1045–55.